Chapter 4

4 DETERMINATION OF THE DEXTROUS WORKSPACE OF THE 6–3 STEWART PLATFORM

4.1 INTRODUCTION

It is of particular importance to be able to compute the fixed orientation and dextrous workspaces of a spatial parallel manipulator. Merlet [4] states that in contrast to common serial link mechanisms with three intersecting wrist joint axes, the (orientationally unconstrained reachable) workspace of a (spatial) parallel manipulator cannot be decoupled in two three-dimensional workspaces characterizing the possible translational and orientational motions. The fixed orientation and dextrous workspaces are however useful projections of the reachable workspace that can easily be presented in a human readable way.

The study of the different workspaces of the 6–3 Stewart platform is continued in this chapter with the objective of determining typical dextrous workspace of practical importance.

The dextrous workspace of the planar Stewart platform is defined in Section 2.6.4.1. The corresponding dexterity requirements for the 6–3 Stewart platform is stated in terms of ranges of rotatability of the orientation angles. In general these dexterity requirements may be specified by the triplet:

$$[\alpha_{min} - \alpha_{max}\,,\ \beta_{min} - \beta_{max}\,,\ \gamma_{min} - \gamma_{max}] \tag{4.1}$$

which indicates that the orientation angles α, β and γ must be able to assume *all* values in the respective ranges $[\alpha_{min} - \alpha_{max}]$, $[\beta_{min} - \beta_{max}]$ and $[\gamma_{min} - \gamma_{max}]$ at *any* point in the associated dextrous workspace denoted by $\boldsymbol{A}[\alpha_{min} - \alpha_{max}\,,\ \beta_{min} - \beta_{max}\,,\ \gamma_{min} - \gamma_{max}]$. This is an extension of, and in agreement with, the notation proposed for the planar case.

For the purpose of this study, the general dexterity requirement (4.1) is restricted to:

$$[\alpha_{fix}\,,\ \beta_{fix}\,,\ \gamma_{min} - \gamma_{max}] \tag{4.2}$$

indicating that only γ must be able to assume *all* values in the range $[\gamma_{min} - \gamma_{max}]$, while α and β must respectively assume the fixed values α_{fix} and β_{fix} at *any* point in the associated dextrous workspace denoted by $\boldsymbol{A}[\alpha_{fix}, \beta_{fix}, \gamma_{min} - \gamma_{max}]$.

4.2 Fixed Orientation Accessible Workspace of the 6–3 Stewart Platform

It was shown in Section 2.6.4.4 that two fixed orientation accessible workspaces may be used to determine the planar dextrous workspace. The same procedure is proposed here for the spatial case, and therefore it is important to be able to determine any specified fixed orientation accessible workspace.

Any fixed orientation requirement for the 6 – 3 Stewart platform, i.e. $[\alpha_{fix}, \beta_{fix}, \gamma_{fix}]$ implies three equalities:

$$\alpha = \alpha_{fix}, \ \beta = \beta_{fix} \ \text{and} \ \gamma = \gamma_{fix} \tag{4.3}$$

These three equality constraints (4.3) correspond to the single equality prescribed for the planar Stewart platform (2.27), and here fix the intermediate coordinates of the 6–3 Stewart platform, i.e.:

$$\mathbf{w} = \begin{bmatrix} w_1 \\ w_2 \\ w_3 \end{bmatrix} = \begin{bmatrix} w_{1\,fix} \\ w_{2\,fix} \\ w_{3\,fix} \end{bmatrix} = \mathbf{w}_{fix} \tag{4.4}$$

Here vertical planes will be used (see Section 3.4.1) to map the fixed orientation accessible workspace of the 6–3 Stewart platform.

Apart from the three equalities fixing the intermediate coordinates (4.4), two additional equalities are needed to specify the search direction of each ray in its associated vertical plane. Equality (3.11) defines the orientation of each vertical plane, and depending on whether the plane is to be mapped starting at the lowest possible or highest possible position of the working point, equality (3.15) or equality (3.18) respectively fixes the direction of the ray in the vertical plane.

Thus the "fixed orientation" accessible workspace in vertical plane i, $(i = 0, 1, 2, ..., N_p)$, making an angle θ_i with the *0X*-axis, may be mapped by solving *modified* optimization problem (i) (see Section 2.6.4.2) for j successive rays $(j = 0, 1, 2, ..., N_R)$. These successive rays emanate from $\mathbf{u}^0$ (3.13) at angular intervals δ. In *modified* optimization problem (i), $\mathbf{h}(\mathbf{u}, \mathbf{s}) = \mathbf{0}$ is given by (3.11) and either (3.15) *or* (3.18), and $\mathbf{w} = \mathbf{w}_{fix}$ is given by (4.4).

4.2.1 Results of the Fixed Orientation Accessible Workspace of the 6–3 Stewart Platform

Corresponding to the horizontally fixed orientation accessible workspace $A[0^\circ]$, that was determined for the planar Stewart platform in Section 2.6.4.3, the "horizontally" fixed orientation accessible workspace $A[0^\circ, 0^\circ, 0^\circ]$ of the 6–3 Stewart platform is mapped here. Figure 4.1 shows the upper and lower isometric views of the boundary $\partial A[0^\circ, 0^\circ, 0^\circ]$ of the three-dimensional fixed orientation accessible workspace $A[0^\circ, 0^\circ, 0^\circ]$ of the 6–3 Stewart platform.

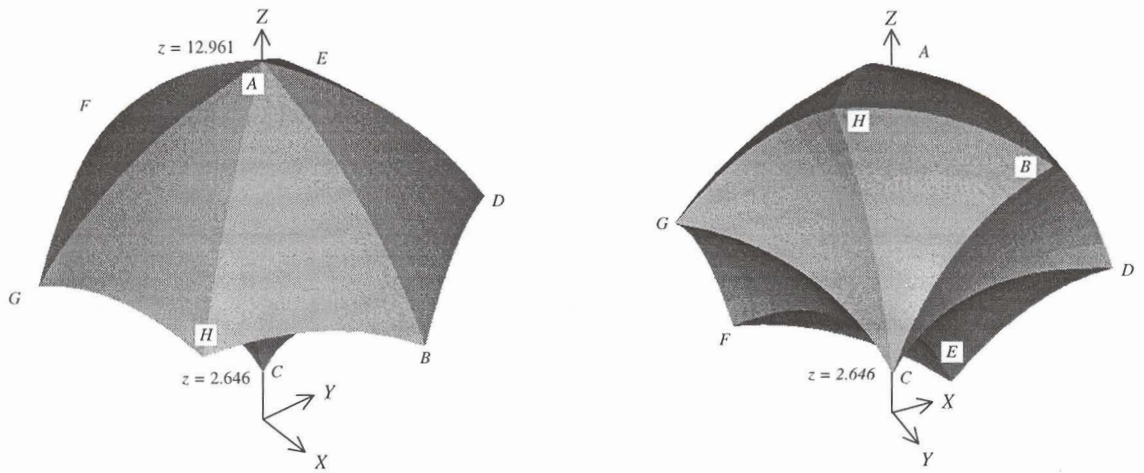

Figure 4.1 Isometric view of the three-dimensional fixed orientation accessible workspace $A[0^\circ, 0^\circ, 0^\circ]$.

The boundary surfaces of $A[0^\circ, 0^\circ, 0^\circ]$ are unique and are independent of whether the vertical planes, used for mapping the workspace, are traced by sweeping from the lowest possible or highest possible working point position.

Note that the lowest possible point ($z = 2.646$) and the highest possible point ($z = 12.961$) on the boundary $\partial A[0^\circ, 0^\circ, 0^\circ]$ and on the *0Z*-axis correspond exactly to the reported (Liu et al. [18]) global coordinates of the working point when all the actuator legs respectively take on their minimum and maximum lengths.

Also note the three fold symmetry of the workspace $A[0^\circ, 0^\circ, 0^\circ]$ about the *0Z*-axis where each third of the workspace spans 120°, and consists of two convex boundary surfaces comprising the upper portion of $A[0^\circ, 0^\circ, 0^\circ]$, and two concave boundary surfaces comprising the lower portion of $A[0^\circ, 0^\circ, 0^\circ]$.

There are also definite bifurcation lines present where the boundary surfaces intersect each other. The vertical bifurcation lines are spaced at 60° rotation intervals, and there are curved "horizontal"

bifurcation lines at the intersection of the upper convex and lower concave boundary surfaces. The previously proposed labeling notation (see Sections 2.5.3 and 2.6.3) is applied to label the fixed orientation accessible workspace $A[0^\circ, 0^\circ, 0^\circ]$.

The proposed optimization approach may be used to map and label the fixed orientation accessible boundary $\partial A[0^\circ, 0^\circ, 0^\circ]$ in any isolated vertical plane i making an angle θ_i with the $0X$-axis. The results for three planes of particular interest, are depicted in Figure 4.2 (a), (b) & (c) for the respective cases: (a) $\partial A[0^\circ, 0^\circ, 0^\circ][\theta_i = 0^\circ]$, (b) $\partial A[0^\circ, 0^\circ, 0^\circ][\theta_i = 30^\circ]$ and (c) $\partial A[0^\circ, 0^\circ, 0^\circ][\theta_i = 60^\circ]$.

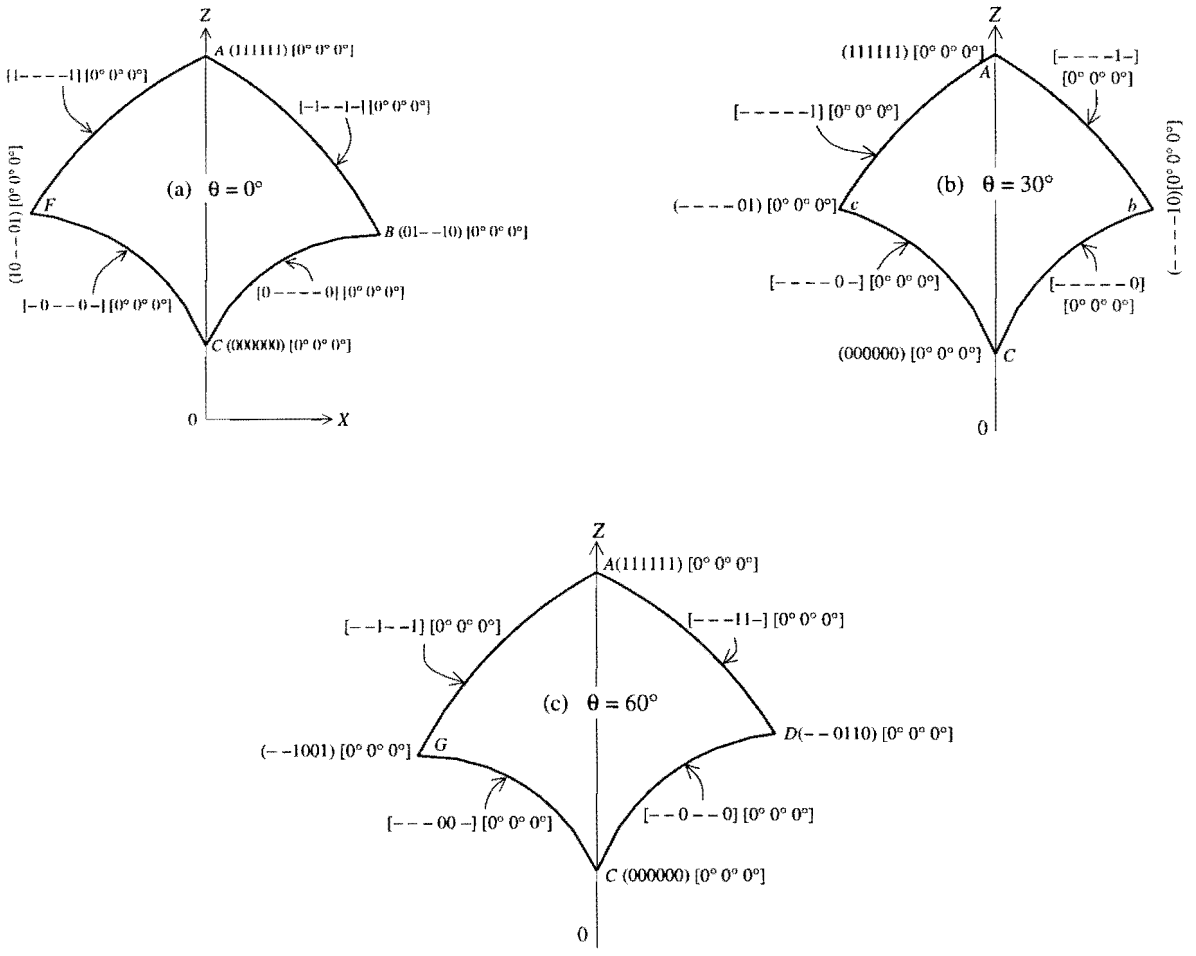

Figure 4.2 $\partial A[0^\circ, 0^\circ, 0^\circ]$ for (a) $\theta_i = 0^\circ$, (b) $\theta_i = 30^\circ$ and (c) $\theta_i = 60^\circ$.

These three vertical sections may be used to describe the behavior of the 6–3 Stewart platform for the working point coinciding with any point on the boundary surfaces defined by the vertices A, B, C and D, as well as the vertices A, F, G and C (see Figure 4.1).

Consider the vertical section through the *0X*-axis at $\theta_i = 0^\circ$, shown in Figure 4.2 (a) together with the related coplanar vertical section *AFC* at $\theta_i = 180^\circ$. It is clear that the lowest possible position of the manipulator working point in $A\,[0^\circ, 0^\circ, 0^\circ]$ is bifurcation point C $(0\ 0\ 0\ 0\ 0\ 0)\ [0^\circ, 0^\circ, 0^\circ]$ where all the actuator legs are at their minimum lengths.

The manipulator working point will follow bifurcation line *CB* $[0 - - - - 0]\ [0^\circ, 0^\circ, 0^\circ]$ as it moves away from its lowest possible position and maintains the fixed orientation $\alpha = 0^\circ, \beta = 0^\circ$ and $\gamma = 0^\circ$. Actuator legs 1 and 6 remain fixed at their minimum lengths while actuator legs 2, 3, 4 and 5 vary. Similarly, bifurcation line *BA* $[- 1 - - 1 -]\ [0^\circ, 0^\circ, 0^\circ]$ represents the path of the manipulator working point with actuator legs 2 and 5 fixed at their maximum lengths, and legs 1, 3, 4 and 6 varying.

Bifurcation point *B* $(0\ 1 - - 1\ 0)\ [0^\circ, 0^\circ, 0^\circ]$ coinciding with the intersection of bifurcation lines *CB* $[0 - - - - 0]\ [0^\circ, 0^\circ, 0^\circ]$ and *BA* $[- 1 - - 1 -]\ [0^\circ, 0^\circ, 0^\circ]$ is the position of the working point if actuator legs 1 and 6 are fixed at their minimum lengths, legs 2 and 5 at their maximum lengths and the top platform fixed in a horizontal orientation (4.4).

Bifurcation point *B* $(0\ 1 - - 1\ 0)\ [0^\circ, 0^\circ, 0^\circ]$ is found by minimizing an error function similar to (2.24) defined in Section 2.6.3.1. Details of the procedure is described in Appendix C.

Finally bifurcation point *A* $(1\ 1\ 1\ 1\ 1\ 1)\ [0^\circ, 0^\circ, 0^\circ]$ is the highest point in the fixed orientation accessible workspace $A\,[0^\circ, 0^\circ, 0^\circ]$, indicating the position of the working point if all the actuator legs at their maximum lengths.

The vertical section at $\theta_i = 180^\circ$ is also shown in Figure 4.2 (a) and is labeled in a similar manner.

Figure 4.2 (b) shows the section of the fixed orientation accessible boundary $\partial A\,[0^\circ, 0^\circ, 0^\circ]$ at $\theta_i = 30^\circ$ (curve *AbC*) and at $\theta_i = 210^\circ$ (curve *AcC*). The concave curve *Cb* $[- - - - - 0]\ [0^\circ, 0^\circ, 0^\circ]\,[\theta_i = 30^\circ]$ is the boundary path of the manipulator working point with leg 6 fixed at its minimum length and the remaining legs varying.

The single leg fixed at its extreme length is due to the fact that *modified* optimization problem (i), specified in terms of the six output and intermediate coordinates, has five equalities defined in Section 4.2. The five equalities comprise of the three equalities given by equation (4.4) and the two additional

equalities needed to specify the search direction of each ray in its associated vertical plane. The displacement from the radiating point $\mathbf{u}^0$ is therefore maximized until the first actuator leg reaches an extreme length resulting in a boundary point on any of the 12 boundary surfaces enclosing the fixed orientation accessible workspace $A\,[0^\circ,\ 0^\circ,\ 0^\circ]$.

Curve *bA* $[-\ -\ -\ -\ 1\ -]\ [0^\circ,\ 0^\circ,\ 0^\circ]\,[\theta_i = 30^\circ]$ carries a similar label. Boundary surfaces *ABD* and *BCD* (see Figure 4.1) may therefore respectively be labeled as *ABD* $[-\ -\ -\ -\ 1\ -]\ [0^\circ,\ 0^\circ,\ 0^\circ]$ and *BCD* $[-\ -\ -\ -\ -\ 0]\ [0^\circ,\ 0^\circ,\ 0^\circ]$.

The above also explains why a bifurcation or intersecting line exists where two bounding surfaces on $\partial A\,[0^\circ,\ 0^\circ,\ 0^\circ]$ intersect. Along this line two actuator legs remain fixed at their extreme values. Similarly the number of legs assuming extreme lengths at any bifurcation point is dependent on the different kinds of boundary surfaces intersecting at the specific bifurcation point.

It is interesting to note that the convex vertical bifurcation lines and convex boundary surfaces are associated with maximum extreme leg lengths, and the concave ones with minimum extreme leg lengths.

A final aspect of interest concerning the fixed orientation accessible workspace $A\,[0^\circ,\ 0^\circ,\ 0^\circ]$ is the bifurcation line *BD* $[-\ -\ -\ -\ 1\ 0]\ [0^\circ,\ 0^\circ,\ 0^\circ]$. The label of this bifurcation line corresponds to the label of point $b\ (-\ -\ -\ -\ 1\ 0)\ [0^\circ,\ 0^\circ,\ 0^\circ]\,[\theta_i = 30^\circ]$ in Figure 4.2 (b). At point $b\ (-\ -\ -\ -\ 1\ 0)\ [0^\circ,\ 0^\circ,\ 0^\circ]\,[\theta_i = 30^\circ]$ six constraints are active, namely the direction of the vertical plane (3.11), the two actuator legs assuming extreme lengths and the three orientation angles (4.4). Point *b* may accordingly be solved for by minimizing the following error function using *LFOPCV3*:

$$\begin{aligned} e(\mathbf{u},\mathbf{w}) = &\left(v_5(\mathbf{u},\mathbf{w}) - v_5^{max}\right)^2 + \left(v_6(\mathbf{u},\mathbf{w}) - v_6^{min}\right)^2 + \left(u_2 - u_1\tan(\theta)\right)^2 \\ &+ (w_1 - 0)^2 + (w_2 - 0)^2 + (w_3 - 0)^2 \end{aligned} \tag{4.5}$$

The labeled bifurcation points, bifurcation lines and boundary surfaces comprising the fixed orientation accessible boundary $\partial A\,[0^\circ,\ 0^\circ,\ 0^\circ]$ shown in Figure 4.1 are:

Bifurcation points:

$A\ (1\ 1\ 1\ 1\ 1\ 1)\ [0^\circ,\ 0^\circ,\ 0^\circ]$ $B\ (0\ 1\ -\ -\ 1\ 0)\ [0^\circ,\ 0^\circ,\ 0^\circ]$ $C\ (0\ 0\ 0\ 0\ 0\ 0)\ [0^\circ,\ 0^\circ,\ 0^\circ]$

$D\ (-\ -\ 0\ 1\ 1\ 0)\ [0^\circ,\ 0^\circ,\ 0^\circ]$ $E\ (1\ 0\ 0\ 1\ -\ -)\ [0^\circ,\ 0^\circ,\ 0^\circ]$ $F\ (1\ 0\ -\ -\ 0\ 1)\ [0^\circ,\ 0^\circ,\ 0^\circ]$

$G\ (-\ -\ 1\ 0\ 0\ 1)\ [0^\circ,\ 0^\circ,\ 0^\circ]$ $H\ (0\ 1\ 1\ 0\ -\ -)\ [0^\circ,\ 0^\circ,\ 0^\circ]$

Bifurcation lines (upper convex):

AB [– 1 – – 1 –] [0°, 0°, 0°] AD [– – – 1 1 –] [0°, 0°, 0°] AE [1 – – 1 – –] [0°, 0°, 0°]

AF [1 – – – – 1] [0°, 0°, 0°] AG [– – 1 – – 1] [0°, 0°, 0°] AH [– 1 1 – – –] [0°, 0°, 0°]

Bifurcation lines (lower concave):

CB [0 – – – – 0] [0°, 0°, 0°] CD [– – 0 – – 0] [0°, 0°, 0°] CE [– 0 0 – – –] [0°, 0°, 0°]

CF [– 0 – – 0 –] [0°, 0°, 0°] CG [– – – 0 0 –] [0°, 0°, 0°] CH [0 – – 0 – –] [0°, 0°, 0°]

Bifurcation lines (horizontally orientated):

BD [– – – – 1 0] [0°, 0°, 0°] DE [– – 0 1 – –] [0°, 0°, 0°] EF [1 0 – – – –] [0°, 0°, 0°]

FG [– – – – 0 1] [0°, 0°, 0°] GH [– – 1 0 – –] [0°, 0°, 0°] HB [0 1 – – – –] [0°, 0°, 0°]

Boundary surfaces (upper convex):

ABD [– – – – 1 –] [0°, 0°, 0°] ADE [– – – 1 – –] [0°, 0°, 0°] AEF [1 – – – – –] [0°, 0°, 0°]

AFG [– – – – – 1] [0°, 0°, 0°] AGH [– – 1 – – –] [0°, 0°, 0°] AHB [– 1 – – – –] [0°, 0°, 0°]

Boundary surfaces (lower concave):

CBD [– – – – – 0] [0°, 0°, 0°] CDE [– – 0 – – –] [0°, 0°, 0°] CEF [– 0 – – – –] [0°, 0°, 0°]

CFG [– – – – 0 –] [0°, 0°, 0°] CGH [– – – 0 – –] [0°, 0°, 0°] CHB [0 – – – – –] [0°, 0°, 0°]

4.3 THE COMPUTATION OF A SPECIFIC SPATIAL DEXTROUS WORKSPACE

The specific dextrous workspace of the 6–3 Stewart platform considered here has the restricted dexterity requirement (4.2):

$$[0^\circ,\ 0^\circ,\ (-30^\circ)-(30^\circ)] \tag{4.6}$$

Here, in accordance with the treatment for the planar case (Section 2.6.4.4), two spatial fixed orientation accessible workspaces, $\boldsymbol{A}[0^\circ,\ 0^\circ,\ -30^\circ]$ and $\boldsymbol{A}[0^\circ,\ 0^\circ,\ 30^\circ]$ are determined. The intersecting or overlapping volume is assumed to be the dextrous workspace $\boldsymbol{A}[0^\circ,\ 0^\circ,\ (-30^\circ)-(30^\circ)]$, within which the full dexterity requirement (4.6) is met at each point enclosed by $\partial\boldsymbol{A}[0^\circ,\ 0^\circ,\ (-30^\circ)-(30^\circ)]$.

Figure 4.3 shows the fixed orientation accessible workspace $A[0^\circ, 0^\circ, -30^\circ]$ with boundary $\partial A[0^\circ, 0^\circ, -30^\circ]$. Note that the highest point in Figure 4.3 is at $z = 10.82$, and the lowest point is at $z = 6.535$.

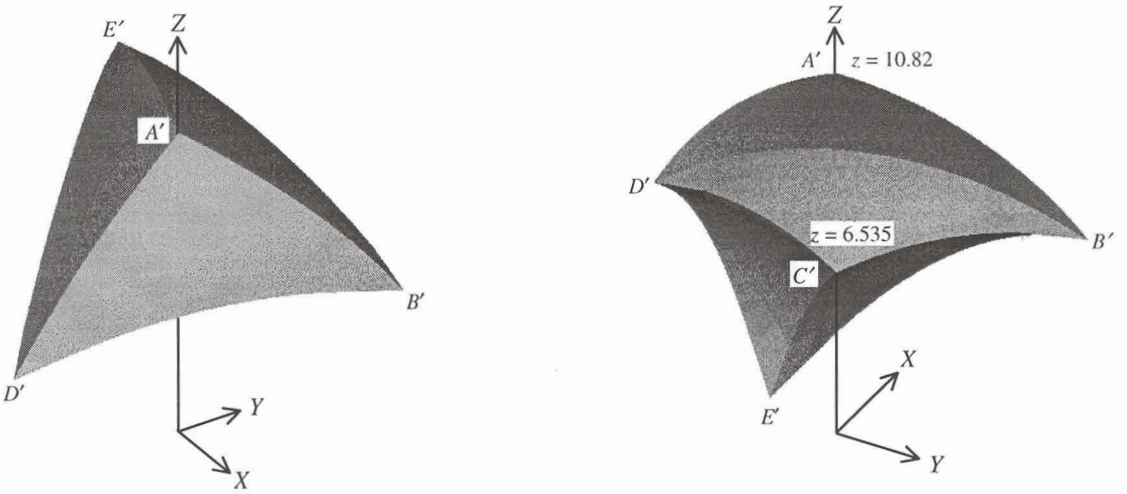

Figure 4.3 Fixed orientation accessible workspace boundary $\partial A[0^\circ, 0^\circ, -30^\circ]$.

The boundary $\partial A[0^\circ, 0^\circ, -30^\circ]$in Figure 4.3 is labeled according to the convention described in Section 4.2.1:

Bifurcation points:

A' (– 1 – 1 – 1) $[0^\circ, 0^\circ, -30^\circ]$ B' (0 1 0 1 – –) $[0^\circ, 0^\circ, -30^\circ]$

C' (0 – 0 – 0 –) $[0^\circ, 0^\circ, -30^\circ]$ D' (0 1 – – 0 1) $[0^\circ, 0^\circ, -30^\circ]$

E' (– – 0 1 0 1) $[0^\circ, 0^\circ, -30^\circ]$

Bifurcation lines (upper convex):

$A'B'$ [– 1 – 1 – –] $[0^\circ, 0^\circ, -30^\circ]$ $A'D'$ [– 1 – – – 1] $[0^\circ, 0^\circ, -30^\circ]$

$A'E'$ [– – – 1 – 1] $[0^\circ, 0^\circ, -30^\circ]$

Bifurcation lines (lower concave):

$C'B'$ [0 – 0 – – –] $[0^\circ, 0^\circ, -30^\circ]$ $C'D'$ [0 – – – 0 –] $[0^\circ, 0^\circ, -30^\circ]$

$C'E'$ [– – 0 – 0 –] $[0^\circ, 0^\circ, -30^\circ]$

Bifurcation lines (horizontally orientated):

$B'D'$ [0 1 – – – –] $[0^\circ, 0^\circ, -30^\circ]$ $D'E'$ [– – – – 0 1] $[0^\circ, 0^\circ, -30^\circ]$

$E'B'$ [– – 0 1 – –] $[0^\circ, 0^\circ, -30^\circ]$

Boundary surfaces (upper convex):

$$A'B'D' \; [-\,1\,-\,-\,-\,-] \; [0^\circ,\, 0^\circ,\, -30^\circ] \quad A'D'E' \; [-\,-\,-\,-\,-\,1] \; [0^\circ,\, 0^\circ,\, -30^\circ]$$

$$A'E'B' \; [-\,-\,-\,1\,-\,-] \; [0^\circ,\, 0^\circ,\, -30^\circ]$$

Boundary surfaces (lower concave):

$$C'B'D' \; [0\,-\,-\,-\,-\,-] \; [0^\circ,\, 0^\circ,\, -30^\circ] \quad C'D'E' \; [-\,-\,-\,0\,-] \; [0^\circ,\, 0^\circ,\, -30^\circ]$$

$$C'E'B' \; [-\,-\,0\,-\,-\,-] \; [0^\circ,\, 0^\circ,\, -30^\circ]$$

The spatial workspace $A\,[0^\circ,\, 0^\circ,\, -30^\circ]$ retains the three-fold symmetry, and possesses three convex and three concave boundary surfaces along the upper and lower portions of the fixed orientation accessible boundary $\partial A\,[0^\circ,\, 0^\circ,\, -30^\circ]$.

The three vertically mapped bifurcation lines formed by the three pairs of intersecting boundary surfaces (convex and concave), are in actual fact no longer perfectly vertical because of the 30° rotation. The exact analyses and determination of the typical non-vertical bifurcation curve $A'B'C'$ is presented in Appendix D.

Keeping in mind that the aim here is to determine the dextrous workspace $A\,[0^\circ,\, 0^\circ,\, (-30^\circ)-(30^\circ)]$, it is required to determine the intersection of the fixed orientation workspace $A\,[0^\circ,\, 0^\circ,\, 30^\circ]$ (Volume $A'C'F'G'H'$ shown in Figure 4.4) with the fixed orientation workspace $A\,[0^\circ,\, 0^\circ,\, -30^\circ]$ (Volume $A'B'C'D'E'$ shown in Figure 4.3 and Figure 4.4). These two fixed orientation accessible workspaces overlap each other as shown in Figure 4.4 and their intersection is taken as the dexterous workspace of interest, namely $A\,[0^\circ,\, 0^\circ,\, (-30^\circ)-(30^\circ)]$ corresponding to Volume $A'C'I'J'K'L'M'N'$.

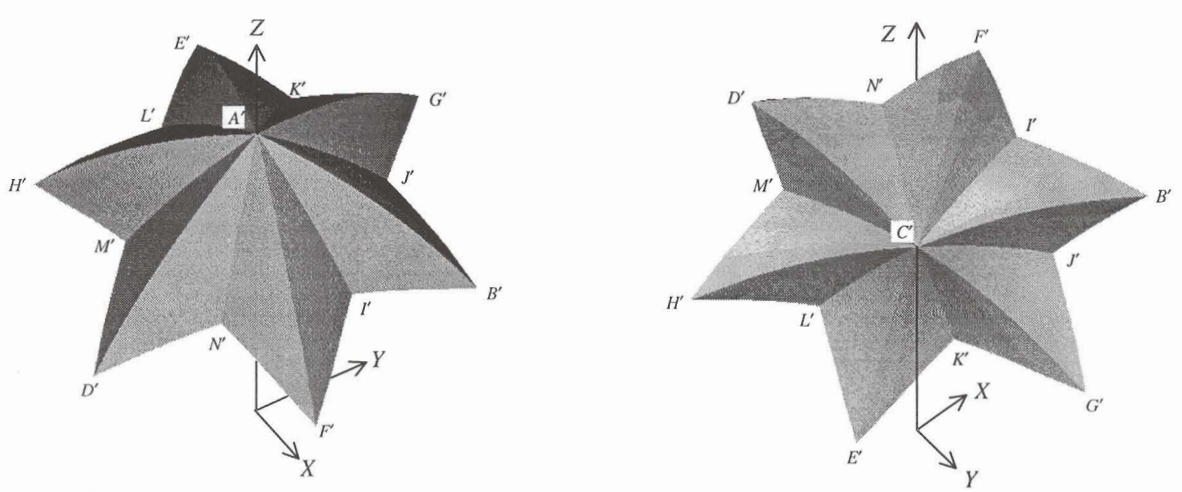

Figure 4.4 Overlap of fixed orientation accessible workspaces $A\,[0^\circ,\, 0^\circ,\, -30^\circ]$ and $A\,[0^\circ,\, 0^\circ,\, 30^\circ]$.

The dextrous workspace found by the intersection of $\boldsymbol{A}\left[0^\circ,\ 0^\circ,\ -30^\circ\right]$ and $\boldsymbol{A}\left[0^\circ,\ 0^\circ,\ 30^\circ\right]$ is depicted in Figure 4.5

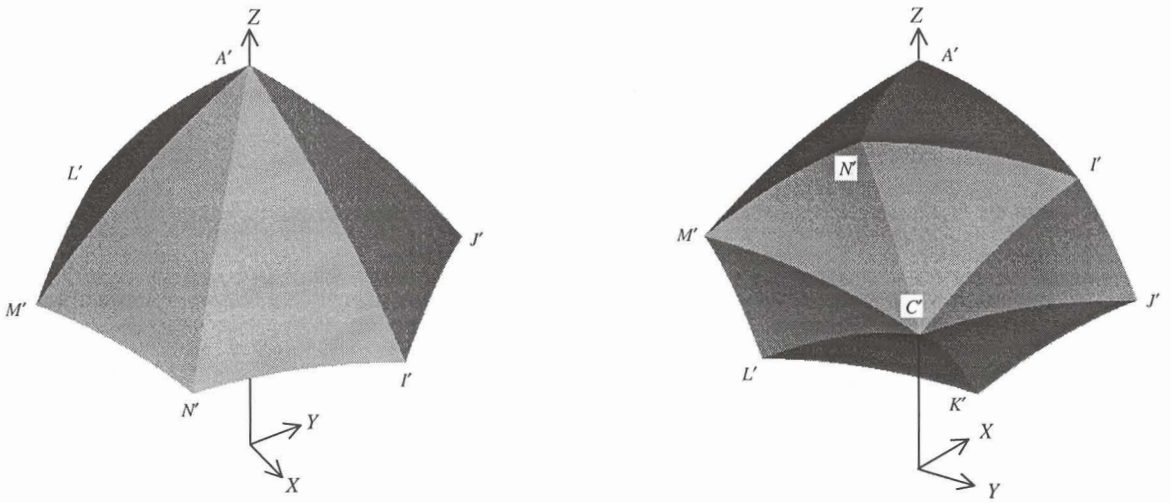

Figure 4.5 The dextrous workspace $\boldsymbol{A}\left[0^\circ,\ 0^\circ,\ (-30^\circ)-(30^\circ)\right]$.

The dextrous workspace is also characterized by the three-fold symmetry about the *0Z*-axis. It is bounded by and consists out of six pairs (convex and concave) of dextrous surfaces separated by six dextrous curves $A'I'C'$, $A'J'C'$, $A'K'C'$, $A'L'C'$, $A'M'C'$ and $A'N'C'$ spaced at 60° intervals. The six dextrous curves are all accurately mapped and carry the same label $\left[0^\circ,\ 0^\circ,\ (-30^\circ)-(30^\circ)\right]$ indicating that the full dexterity requirement is met along these curves.

Figure 4.6 shows sections of the dextrous boundary $\partial\boldsymbol{A}\left[0^\circ,\ 0^\circ,\ (-30^\circ)-(30^\circ)\right]$ mapped in the vertical plane at $\theta_i = 0^\circ$ and $\theta_i = 180^\circ$.

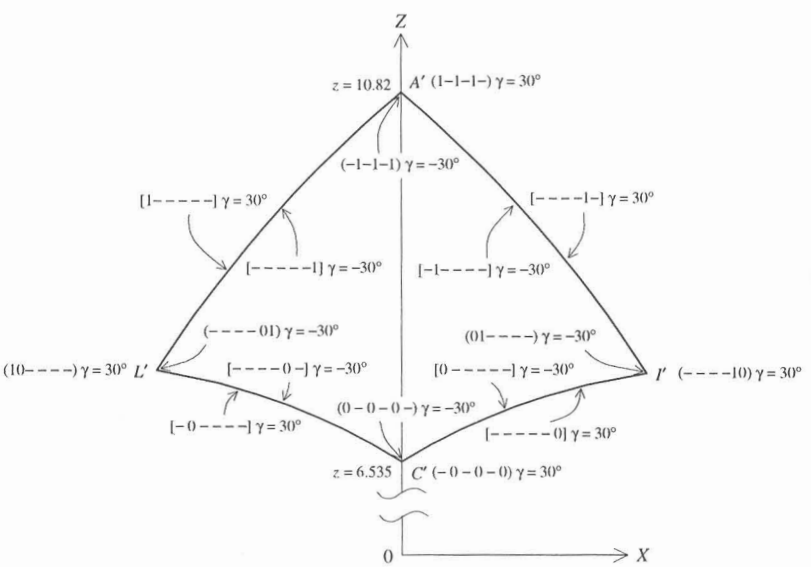

Figure 4.6 Sections of the dextrous boundary $\partial\boldsymbol{A}\left[0^\circ,\ 0^\circ,\ (-30^\circ)-(30^\circ)\right]$ at $\theta_i = 0^\circ$ and $\theta_i = 180^\circ$.

This boundary was mapped as two fixed orientation accessible boundaries $\partial A\left[0^\circ,\ 0^\circ,\ -30^\circ\right]$ and $\partial A\left[0^\circ,\ 0^\circ,\ 30^\circ\right]$ and they coincide exactly as shown in Figure 4.6. The same behavior is also evident at the other vertical dextrous curves separating the dextrous boundary surfaces which makes it easy to map sections of the dextrous workspace as shown in Figure 4.6.

With reference to Figure 4.4, the convex dextrous boundary surface $A'I'J'\ \left[0^\circ,\ 0^\circ,\ (-30^\circ)-(30^\circ)\right]$ forms part the fixed orientation accessible boundary surface $A'F'G'\ \left[0^\circ,\ 0^\circ,\ 30^\circ\right]$. The concave dextrous boundary surface $C'I'J'\ \left[0^\circ,\ 0^\circ,\ (-30^\circ)-(30^\circ)\right]$ forms part of the fixed orientation accessible boundary surface $C'F'G'\ \left[0^\circ,\ 0^\circ,\ 30^\circ\right]$. This implies that the first 60° of the dextrous workspace boundary $\partial A\left[0^\circ,\ 0^\circ,\ (-30^\circ)-(30^\circ)\right]$ may be found by mapping the first 60° of the fixed orientation accessible workspace $A\left[0^\circ,\ 0^\circ,\ 30^\circ\right]$.

Similarly, the convex dextrous boundary surface $A'J'K'\ \left[0^\circ,\ 0^\circ,\ (-30^\circ)-(30^\circ)\right]$ forms part of the fixed orientation accessible boundary surface $A'B'E'\ \left[0^\circ,\ 0^\circ,\ -30^\circ\right]$. The concave dextrous boundary surface $C'J'K'\ \left[0^\circ,\ 0^\circ,\ (-30^\circ)-(30^\circ)\right]$ forms part of the fixed orientation accessible boundary surface $C'E'B'\ \left[0^\circ,\ 0^\circ,\ -30^\circ\right]$. The dextrous boundary $\partial A\left[0^\circ,\ 0^\circ,\ (-30^\circ)-(30^\circ)\right]$ spanning $\theta_i = 60^\circ$ to $\theta_i = 120^\circ$ may therefore be found by mapping the corresponding range ($\theta_i = 60^\circ$ to $\theta_i = 120^\circ$) of the fixed orientation accessible workspace $A\left[0^\circ,\ 0^\circ,\ -30^\circ\right]$. In practice the intersection of the two fixed orientation workspaces is relatively easy to compute.

The three fold symmetry of the dextrous workspace $A\left[0^\circ,\ 0^\circ,\ (-30^\circ)-(30^\circ)\right]$ also necessitates only the first 120° be mapped.

The validity of assumption (2.30) in Section 2.6.4.4, and applied here to the spatial case, is shown in Figure 4.7, where the different fixed orientation accessible workspaces determined in this chapter are placed at an X-offset next to each other. The dextrous workspace $A\left[0^\circ,\ 0^\circ,\ (-30^\circ)-(30^\circ)\right]$ clearly satisfies condition (2.31) of Section 2.6.4.4.

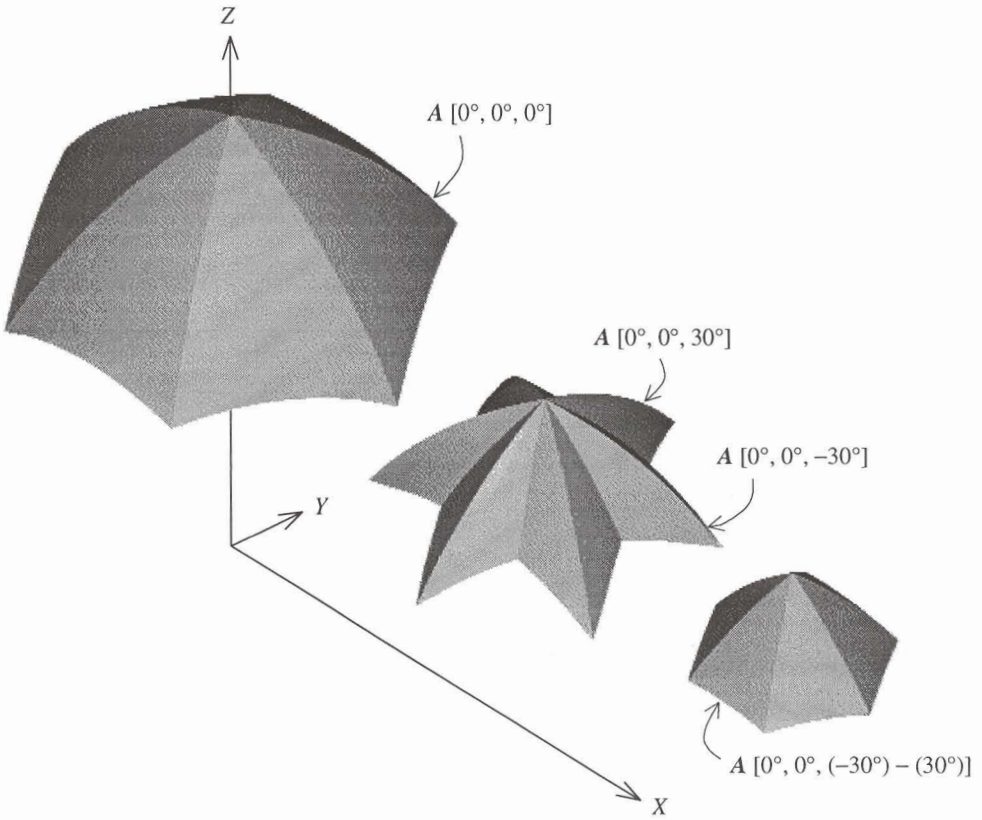

Figure 4.7 $A[0^\circ, 0^\circ, 0^\circ]$, the overlap of $A[0^\circ, 0^\circ, -30^\circ]$ and $A[0^\circ, 0^\circ, 30^\circ]$ and the final dextrous workspace $A[0^\circ, 0^\circ, (-30^\circ)-(30^\circ)]$.